Defence Science Journal, Vol. 65, No. 4, July 2015, pp. 279-286, DOI : 10.14429/dsj.65.8648

Numerical Simulation on Jet Formation of Shaped Charge with Different Liner Materials

Cheng Wang*, Jianxu Ding, and Haitao Zhao

State Key Laboratory of Explosion Science and Technology, Beijing Institute of Technology, Beijing-100 081, China
**E-mail: wangcheng@bit.edu.cn*

ABSTRACT

In this paper, the effect of liner material of the shaped charge on jet formation and its penetration capability is investigated by experimental and numerical methods. Liner materials investigated in this paper are copper, steel, and aluminium, respectively. Pulse X-ray photographic technology to shoot the formation of jet is employed to obtain the tip velocity and the diameter of jet. A two-dimensional multi-material code is designed to simulate the entire process from jet formation to penetrating a target. A markers on cell lines method is utilised to treat the multi-material interface. The results show that aluminium jet has the highest velocity with the poorest penetration capability. Copper jet has the strongest penetration capability with a velocity higher than that of steel jet, but lower than that of aluminium jet. The simulated results agree with the experimental results very well. It also indicates that the code developed can not only address large distortion problems but also track the variation of multi-material interfaces. It is favourable to simulate the explosive loading on thin-wall structure such as shaped charge. It is proved that authors' method is feasible and reliable for optimising the structure of shaped charge jet to dramatically improve its tip velocity and penetration capability, and provides an important theoretic basis for designing high explosive anti-tank warhead.

Keywords: Shaped charge, jet, liner material, penetration, numerical simulation

1. INTRODUCTION

Shaped charges are explosive charges that are specially designed to produce powerful metal jet causing stronger penetration effects onto hard targets, which is important for military and industrial applications[1]. A shaped charge is generally a cylinder of high explosive with a cavity in one end lined with a thin layer of metal, and a detonator at the opposite end. Upon initiation a detonation wave propagates through the explosive charges and further impinges on the liner to the axis of symmetry. The inner layer of material forms a high velocity jet, while the remainder of the materials forms a low velocity slug. By optimizing explosive charge types, geometric configurations, initiation mode, and liner materials for shaped charge, a long, non-fragmented, and high density jet could be obtained to enhance the jet penetration capability[2-4]. Generally speaking, early works on the design of shaped charges were inspired by trial-and-error experiments. With the development of computer, numerical simulations on shaped charges receive significant attention in recent years[5]. Wave propagation hydrocodes have been tried to simulate shaped charge detonations to predict the behaviour of shape charges [6]. But the ability of penetration into the target was not considered integrally. Huerta[7], *et al.* designed and analyzed shaped charges using CTH hydrocodes to generate a large hole in hard targets. However, the CTH code used contains two step algorithms; first step is a Lagrangian and the second step must redefines the computational meshes making the distorted cells map back to the Eulerian mesh. Lee designed a good shaped charge using a 2-D Eulerian code to create a large hole in the well casing and a small hole in the gun pipe[8]. Molinari developed a finite element Lagrangian code to simulate the formation, the fragmentation and penetration of shaped charge jet[9]. But, in his finite element Lagrangian code, the rubber replaced explosive and using a heavy impacting mass represented the detonator. Chen[10], *et al.* utilized the improved CE/SE scheme combining with a high-resolution interface tracking method and a ghost fluid type boundary treatment to simulate shaped charge jetreliably. But they did not compare the computing results such as kinetic energy of the jet and velocity gradient with the relevant experiments. Baêta-Neves[11], *et al.* simulated the detonation process of a cylinder-shaped charge using the 2-D smoothed particle hydrodynamics (SPH) procedure in cylindrical coordinates. However, the interfacial treatment used in their simulations failed to exactly describe the interaction of detonation wave with the liner, which produced some difference between the numerical and experimental results. Ma[12], *et al.* developed a three-dimensional MPM3DPP code using adaptive MPM to simulate shaped charge problems. Wang[13], *et al.* developed a two-dimensional hydro-elasto-plastic code with multi-material interface reconstruction to simulate jet formation. Johnston[14], *et al.* used AUTODYN to identify the jetting behaviors in the explosion process of linear

Received 06 April 2015, revised 10 July 2015, online published 30 July 2015

shaped charges and the peculiar flight of the jet impacting a target. Wojewodka[15], *et al.* used LS-DYN software to simulate the jet formation process in a linear shaped charge. Although commercial codes such as AUTODYN and LS-DYN can simulate the whole process of the jet formation and penetration, the results obtained cannot reach the high resolution. A high-fidelity numerical computation, the LLNL's advanced multi-physics hydrodynamics code (ALE3D), was performed by Scott Stewart[16], *et al.* to study the process of micro-shaped charge jet formation and penetration depth. By the numerical and experimental approaches, Liang[17], *et al.* investigated the effects of shaped charge jet on penetration into targets. Because their code was unable to compute the overall process of jet formation and penetration, they made an assumption that sharped charge jet was a high speed kinetic energy rod with a large velocity gradient. Although a large number of codes have been developed and used to simulate shaped charges, there are few reports investigating the effects of explosive charge types, geometrical configurations and especially different liner materials on jet formation and its penetration capability.

Numerical simulation of shaped charges includes four basic processes: high explosive detonation, liner collapse, jet formation, and target penetration. In this study, instead of simulating separately, all four processes are integrated together and simulated by using a two dimensional multi-material code. The effects of different liner materials on jet formation and target penetration are investigated. To confirm the simulation results, experiments employing pulse X-ray photograph technology to shoot jet formation process of different liner material are performed. The simulated results are in agreement with experimental results very well. It indicates that the code can not only simulate large deformation problem, but also clearly track the evolution of the multi-material interfaces. Such a numerical simulation approach is of great significance for engineering applications to optimize the design of shaped charge.

2. JET FORMATION EXPERIMENTS AND ANALYSIS OF THE RESULTS

In this experiment, the liner materials for shaped charge is OFHC copper and 1045 steel, respectively. Because aluminium density is too small, the X-ray pictures can't clearly show the jet formation process with aluminium as the liner material. Composition B is chosen as the main charge. Its density was 1.666 g/cm^3 and the detonation velocity was 8,221 m/s. The diameter of the shaped charge is 60 mm, the total height of the charge is 75.3 mm and the cone angle of the liner is 60°. The liner wall thickness was uniformly 2.4 mm. Pulse X-ray testing system as shown in Fig. 1(a) is employed to shoot the process of jet formation of the shaped charge with steel and copper as the liner material. Figure 1(b) shows the schematic of experimental installation. Figure 2 shows the appearance of the shaped charge jet with steel liner and copper liner, respectively. Table 1 lists the experimental results of the shaped charge jet. In the X-ray pictures, as shown in Fig. 2, the jets are divided and numbered 1, 2, 3, 4, 5, and 6 from top to bottom. The diameters of the jets in each division are measured according to appropriate scales, which are shown in Table 2.

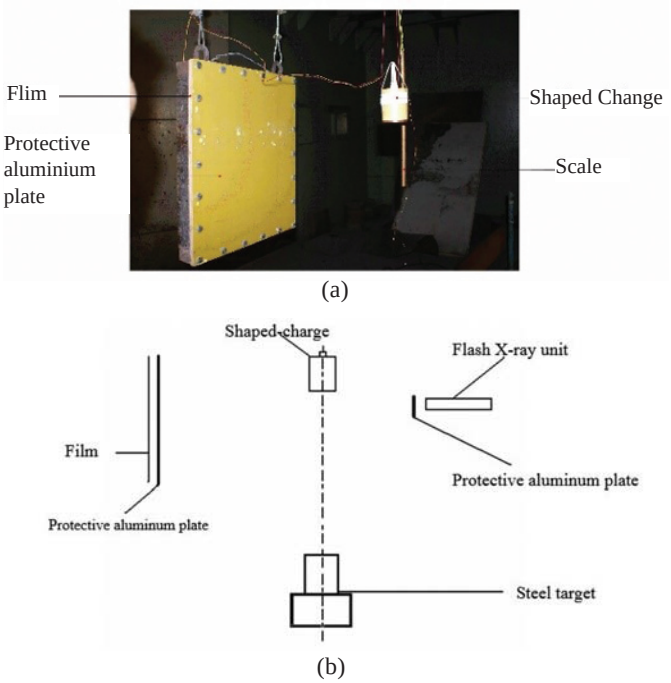

Figure 1. Experiment setup: (a) Pulse X-ray, and (b) Schematic.

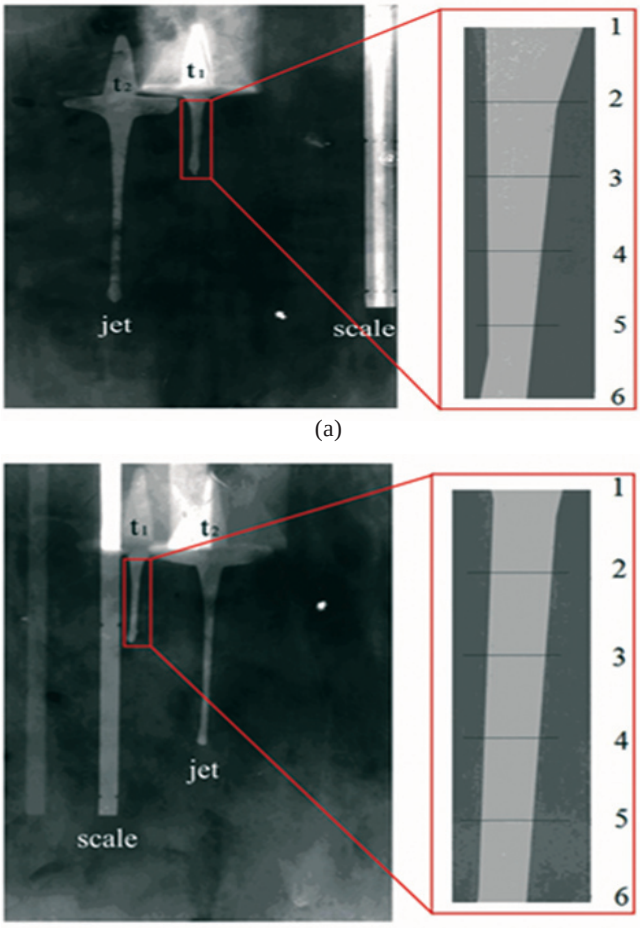

Figure 2. Appearances of shaped charge jet with (a) steel liner and (b) copper liner, as shown in Table 1.

Table 1. Experimental results of jet formation

Parameters	Time t_1 (μs)	Time t_2 (μs)	Tip velocity (m/s)	Tail velocity (m/s)	Length of jet at t_1(mm)	Length of jet at t_2(mm)
Steel	25.5	41.4	5275.2	1321.1	41.2	77.5
Copper	25.6	36.5	5534.6	1363.2	37.1	67.6

Table 2. Experimental results of jet diameters

Material	Diameter at No. 1 (mm)	Diameter at No. 2 (mm)	Diameter at No. 3 (mm)	Diameter at No. 4 (mm)	Diameter at No. 5 (mm)	Diameter at No. 6 (mm)
Steel	6.39	4.79	4.14	3.55	3.11	3.05
Copper	4.64	3.98	3.77	3.57	3.36	3.21

Through analysis of the experimental results, it is found that the tip and tail velocities of the jet produced by both liners are above 5.2 km/s and 1.3 km/s. However, both the tip and tail velocities with copper liner are larger. The diameters of the jet tip produced by both materials are close. However, the variation gradient of the diameter of steel jet is bigger than that of copper jet. At time t_2, steel jet suffers from fracture, but copper jet still remains continuous. Although the time t_2 when the X-ray picture of copper jet is taken is several microseconds earlier than that when the X-ray picture of steel jet is taken, the main reason is because that copper has good tensile properties and larger ductility under tension. Larger ductility results in a longer jet, which can enhance its penetration capability.

3. NUMERICAL COMPUTATION

To understand the principles of shaped charges and evaluate the designs, the whole process including detonation wave propagating and interacting with the liner, jet forming and penetrating the target and crater forming in the target has to be simulated. This complicated process involves large deformations. By the two-dimensional Euler hydro-elasto-plastic code with multi-material interface treatment, the entire physical process mentioned above is simulated.

3.1 Governing Equations

The governing equations usually include conservation equations, material constitutive model and equation of state.

(i) Conservation equations

$$\frac{\partial \rho}{\partial t}+u_z\frac{\partial \rho}{\partial z}+u_r\frac{\partial \rho}{\partial r}+\rho\left(\frac{\partial u_z}{\partial z}+\frac{\partial r u_r}{r\partial r}\right)=0 \tag{1}$$

$$\rho\left(\frac{\partial u_z}{\partial t}+u_z\frac{\partial u_z}{\partial z}+u_r\frac{\partial u_z}{\partial r}\right)=-\frac{\partial P}{\partial z}+\frac{\partial S_{zz}}{\partial z}+\frac{\partial r S_{rz}}{r\partial r} \tag{2}$$

$$\rho\left(\frac{\partial u_r}{\partial t}+u_z\frac{\partial u_r}{\partial z}+u_r\frac{\partial u_r}{\partial r}\right)=-\frac{\partial P}{\partial r}+\frac{\partial S_{rz}}{\partial z}+\frac{\partial r S_{rr}}{r\partial r}+\frac{\left(S_{rr}+S_{zz}\right)}{r} \tag{3}$$

$$\rho\left(\frac{\partial e}{\partial z}+u_z\frac{\partial e}{\partial z}+u_r\frac{\partial e}{\partial r}\right)=-P\left(\frac{\partial\left(ru_r\right)}{r\partial r}+\frac{\partial u_z}{\partial z}\right)+S_{zz}\frac{\partial u_z}{\partial z}+S_{rr}\frac{\partial u_r}{\partial r}+S_{rz}\left(\frac{\partial u_z}{\partial r}+\frac{\partial u_r}{\partial z}\right)-\frac{u_r\left(S_{rr}+S_{zz}\right)}{r} \tag{4}$$

where t represents time; r and z are Euler coordinates; u_r and u_z are the velocity components in the respective r and z directions; p, ρ and e are pressure, density and specific internal energy, respectively; S_{rr}, S_{zz}, and S_{rz} are deviatoric stresses, respectively.

(ii) Material constitutive model

Within the range of elasticity, the general Hooke principle is adopted as follows

$$S_{rr}=2G\left(\varepsilon_{rr}-\frac{1}{3}\mu\right)+\delta_{rr},\ S_{zz}=2G\left(\varepsilon_{zz}-\frac{1}{3}\mu\right)+\delta_{zz},\ S_{rz}=2G\varepsilon_{rz}+\delta_{rz} \tag{5}$$

by definition,

$$\dot{\varepsilon}_{rr}=\frac{\partial u_r}{\partial r},\ \dot{\varepsilon}_{zz}=\frac{\partial u_z}{\partial z},\ \dot{\varepsilon}_{rz}=\frac{1}{2}\left(\frac{\partial u_z}{\partial r}+\frac{\partial u_r}{\partial z}\right),$$

$$\dot{\mu}=\frac{\partial\left(ru_r\right)}{r\partial r}+\frac{\partial u_z}{\partial z}$$

where δ_{zz}, δ_{rz}, δ_{rr} are correction factors for rigid body rotation.

To check whether a material is in elastic state or plastic state, von Mises criterion is used. When the second invariant of stress deviator meets the following formula, the material yields

$$S_{rr}^2+S_{zz}^2+S_{rz}^2+S_{rr}S_{zz}=\frac{1}{3}Y_0^2 \tag{6}$$

For the stress-strain relationship in the ideal plastic state, an approximation equation is used. Namely, the stress deviators are derived from elastic stress-strain relationship, and then the plasticity is corrected[18].

$$\beta_1=\sqrt{Y_0^2\Big/\left(3\left(S_{rr}^2+S_{zz}^2+S_{rz}^2+S_{rr}S_{zz}\right)\right)} \tag{7}$$

when $\beta_1<1$, plastic state is produced, so the stress deviators are revised as

$$S'_{rr}=\beta_1 S_{rr},\ S'_{zz}=\beta_1 S_{zz},\ S'_{rz}=\beta_1 S_{rz}$$

(iii) Equation of state

The energy released from the high explosive is treated as a programmed burn with a JWL Equation of state[8]

$$P_s=A\exp\left(-R_1V\right)+B\exp\left(-R_2V\right)+CV^{-(\omega+1)} \tag{8}$$

where P_s is the pressure, V is the specific volume, the subscript s indicates isentropic process, and A, B, C, R_1, R_2, ω are constants. The JWL EOS parameters for Composition-B

explosive[8] are taken as: A = 1141.8 GPa; B = 23.9143 GPa; C = 3.3621 GPa; R1 = 5.70; R2 = 1.65; ω = 0.60.The detonation parameters for Composition-B explosive[8] are taken as: Density = 1.666 g/cm^3; pressure = 28.0 GPa; velocity = 8221 m/s; heat = 10.132 kJ/cm^3; Adiabatic exponent = 3.02.

For the liner material, Mie-Grüneison EOS can be expressed in the following form as[19]

$$P = P_H\left(1-\frac{\Gamma\mu}{2}\right)+\Gamma\rho e \tag{9}$$

$$P_H = \begin{cases}\rho_0 C^2\left(\mu+(2S-1)\mu^2+(3S^2-4S+1)\mu^3\right) & \mu \geq 0\\ \rho_0 C^2\mu & \mu<0\end{cases} \tag{10}$$

where the subscript H refers to the Hugoniot curve and Γ is the Mie-Grüneison coefficient. C refers to the bulk sound speed and S is the Hugoniot slop coefficient. The parameters[19] for Mie-Grüneison EOS are shown in Table 3.

3.2 Computation Method

An operator splitting method is utilized here to perform the computation. The first step is a Lagrange step. In this step, only the influences of pressure gradient and deviatoric stresses are taken into account to obtain the median velocity and internal energy of grids. The second step is remapping computation. In this step, pure grids are transported by the MUSCL high-resolution scheme with second-order accuracy. For mixed and free-face grids, the MOCL method[13] is applied. Such interface treatment approach can automatically calculate the topographic changes of interfaces, and ensures mass conservation. They are the key techniques for the numerical simulation of jet elongation and penetration.

4. NUMERICAL INVESTIGATIONS ON JET FORMATION WITH DIFFERENT LINER MATERIALS

4.1 Computational Model

The computational domain is split into 600×220 rectangular grids. For the liner material, steel, copper and aluminium are selected. The computational geometric model for the numerical simulation is shown in Fig. 3. Figure 3(a) is the schematic diagram of a shaped charge structure and Fig. 3(b) is the charge dimension. Initiation modes are both plane initiation.

4.2 Computational Results and Analysis

Figures 4(a) - 4(c), respectively show the jet formation process for different liner materials. It can be observed that, when the detonation products push the liner axially, the liner

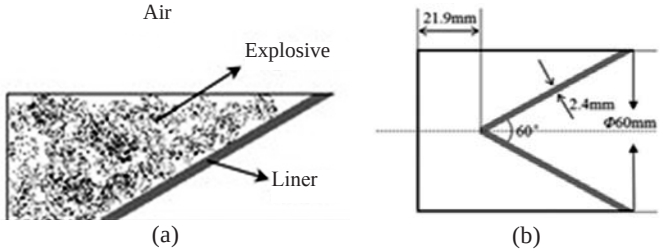

Figure 3. Computational model: (a) Schematic diagram of shaped charge structure and (b) The charge dimension.

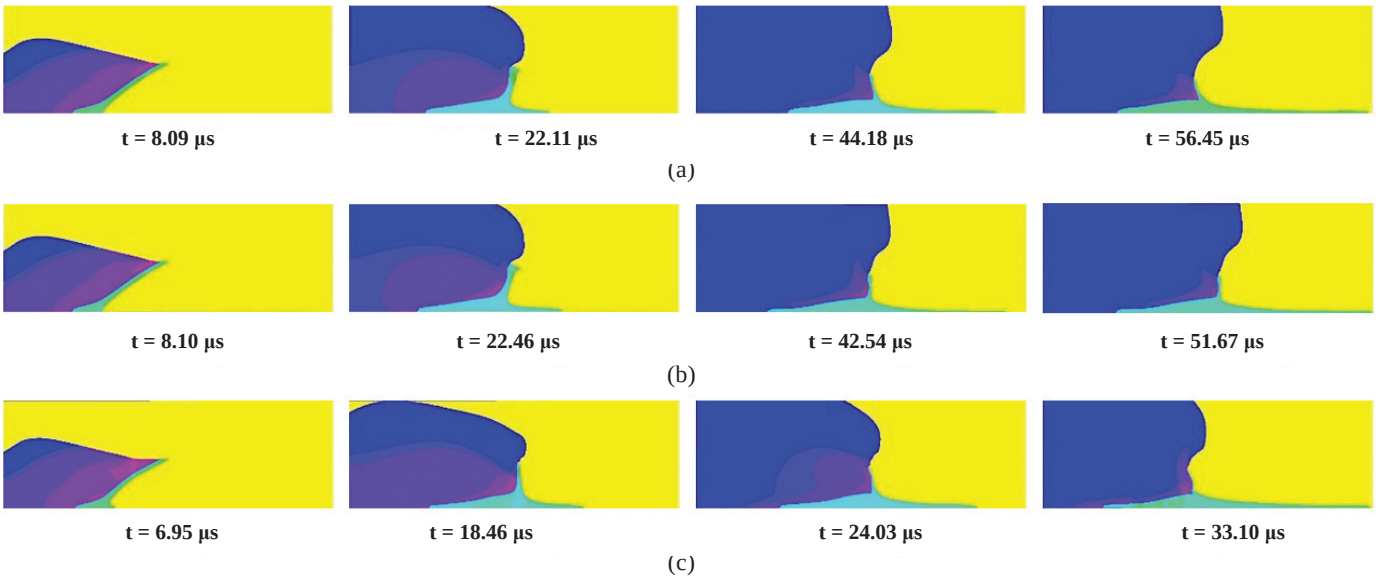

Figure 4. Process of jet formation of: (a) Steel liner shaped charge, (b) Copper liner shaped charge, and (c) Aluminium liner shaped charge.

Table 3. Material property parameters of three kinds of liners

Material	ρ_0(g/cm^3)	C (cm/μs)	S	Y_0 (GPa)	T	Elongation
Steel	7.89	0.36	1.80	0.50	1.81	16%
Copper	8.93	0.39	1.50	0.45	2.00	30-50%
Aluminium	2.71	0.53	1.50	0.55	1.70	11%

wall continuously thickens. It is because the liner is shrunk to an area with a smaller diameter. Afterwards, the liner wall converges and collides at the central axis. At the same time, the material on the internal wall of the liner with higher axial velocity squeezes out along the axis and forms jet; while the material on the exterior wall occupying the majority of mass achieves lower velocity and forms slug.

The numerical and experimental velocities and sizes of the jet with steel and copper liner, respectively, are compared in Tables 4 and 5. From the tables, it can be seen that, the numerical results are in good agreement with the experiment results. The simulated jet tip velocity and jet length at 33.1 μs produced by all three materials are listed in Table 6. The computed diagram of jet formed at this moment is shown in Fig. 5.

From the above numerical results, it can be observed that, under the same conditions, the jet produced by aluminium liner has the largest tip velocity and the biggest length. The jet tip velocity and jet length with copper liner are similar to that of steel jet but a little bit higher. This is because that among the three materials, aluminium has the smallest density and yield stress. It can produce the jet with the highest velocity. Comparing copper and steel, although the density of copper is a bit higher than that of steel, its yield stress is only about one fourth of that of steel. Therefore, the jet velocity with copper liner is bigger than that with steel liner.

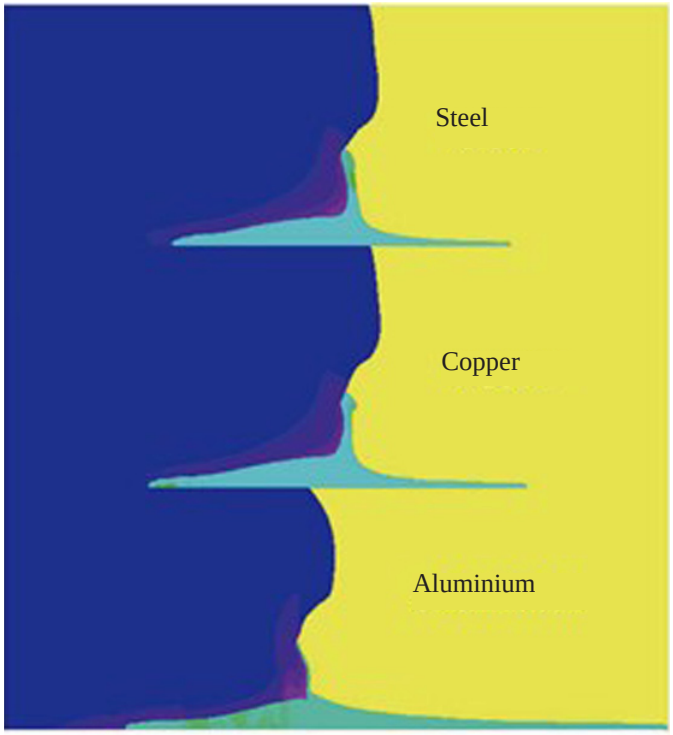

Figure 5. Comparison diagrams of jet produced by different liner materials at time 33.1 μs.

Figure 6 illustrates the variation curve of tip velocity of the jet with time. Initiation of explosive is taken as starting time point. The jet is formed at time 4 μs. After jet forms, the velocities of the elements in the centre are faster than those on the sides. These elements extend from the symmetry axis and move forward. Therefore, the tip of the jet gradually expands. Because the jet elements formed on the liner top are surpassed by the subsequent jet elements with higher velocities, its tip velocity increases. Its tip velocity reaches the maximum value at time 10 μs. After that it decreases gradually. It is explained by the fact that the elements at the tip of the jet homogenize with the other slower jet elements. This process forces the elements at the tip to consume plastic deformation energy, causing the tip velocity of the jet to decrease. Another reason is perhaps that the tip of the jet interacts with air, which further consumes and dissipates plastic deformation energies, causing the tip velocity of the jet to decrease.

For different materials, the liners with the cone angles of both 90° and 120° are also investigated in this paper. It can be

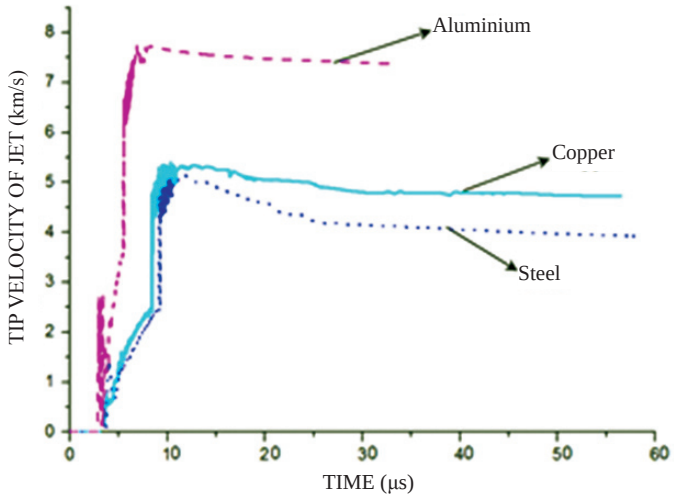

Figure 6. Variation curve of tip velocity of jet with time.

Table 4. Comparison between numerical results and experimental ones for steel jet parameters

Parameters	Tip velocity (m/s)	Tail velocity (m/s)	Jet length at 25.5 μs (mm)	Jet length at 41.4 μs (mm)	Diameter of jet (mm)
Experimental results	5275.2	1321.1	41.2	77.5	4.2
Numerical results	5158.3	1280.3	38.3	74.7	3.9

Table 5. Comparison between numerical results and experimental ones for copper jet parameters

Parameters	Tip velocity (m/s)	Tail velocity (m/s)	Jet length at 25.6 μs (mm)	Jet length at 36.5 μs (mm)	Diameter of jet (mm)
Experimental results	5534.6	1363.2	37.1	67.6	3.7
Numerical results	5395.6	1332.6	35.7	65.3	3.6

seen from Fig. 7 that, with the increase of the cone angle, the tip velocity of shaped charge jet decreases gradually. For the same material, the larger the jet velocity is, the deeper it will penetrate. Based on the penetration depth of sharped charge jet into armour steel, the liner with 60° is investigated in the following subsection.

Table 6. Numerical results of jets produced by different liner materials at time 33.1 μs

Parameters	Steel	Copper	Aluminium
Tip velocity (m/s)	5158.3	5395.6	8136.0
Jet length (mm)	55.7	62.3	130.4

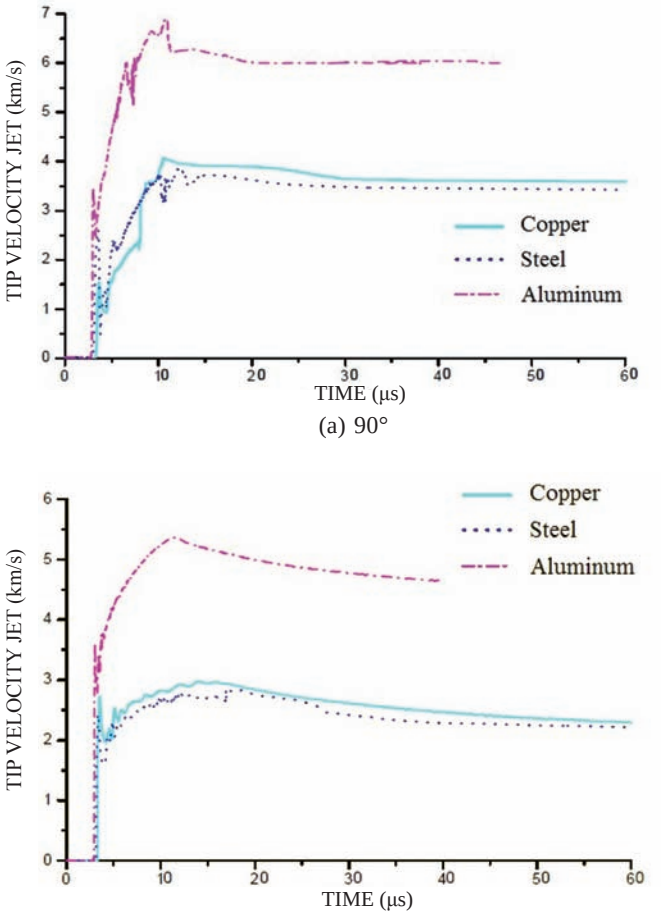

Figure 7. Variation curve of tip velocity of jet with time.

5. NUMERICAL INVESTIGATIONS ON JET PENETRATION WITH DIFFERENT LINER MATERIALS

5.1 Computational Model

Computation of jet penetrating a target is performed based on jet formation. The computation results show that at the time when the jet tip is pulled to 100 mm to the mouth of the liner, detonation products only impose slight influence on the jet formation. Therefore, at this time the detonation products in the computational domain are removed. Then, a 35 mm thick steel target is included in the computation domain, which is put at a position about 100 mm away from the mouth of the liner. The number of grids is still 600 × 220. Then, after the computational domain is reinitiated, simulation of the jet produced by the shaped charge penetrating a target is performed.

5.2 Computational Results and Analysis

Figure 8(a) -8(c), respectively give the penetration process into a steel target by steel, copper and aluminium jets. The numerical results are shown in Table 7.

In Table 7, impact velocity is the tip velocity of the jet at impact and the residual velocity is the tip velocity of the jet after it penetrates through the target. The unit velocity drop average over the penetrating time and the diameter of the hole in the target are important parameters to evaluate the penetration capability of a jet.

Table 7. Numerical results of jet penetrating into steel target

Material	Impact velocity (m/s)	Residual velocity (m/s)	Unit velocity drop average over penetrating time (m/s/μs)	Hole diameter (mm)
Steel	3933.3	1918.4	63.6	9.6
Copper	4781.8	4165.8	29.9	9.4
Aluminium	7827.8	4278.6	233.5	8.4

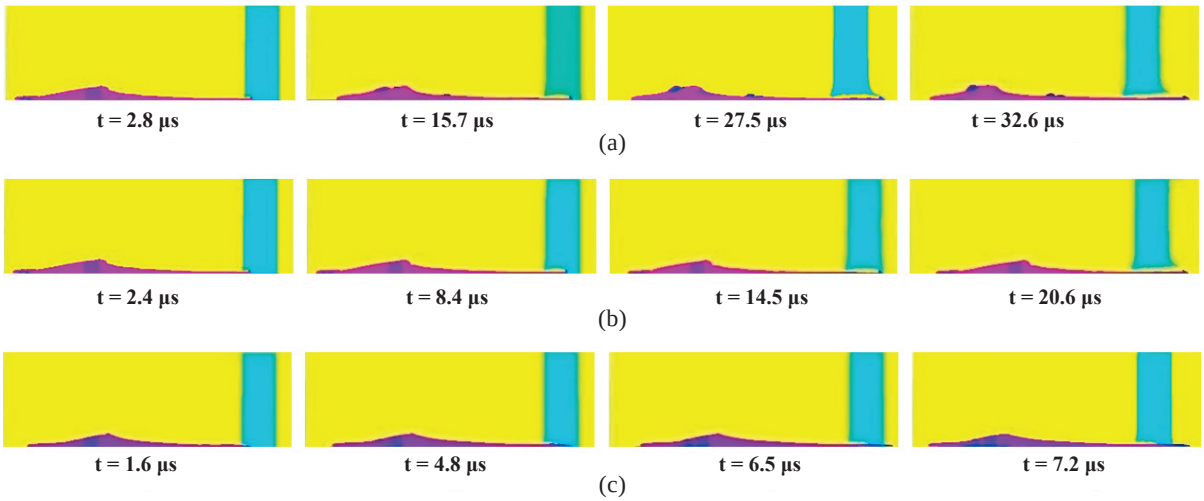

Figure 8. Penetration process of: (a) Steel jet, (b) Copper jet, and (c) Aluminium jet.

It can be seen from Table 7 that, copper jet has the smallest velocity drop within unit time, which is about 29.9 m/s per μs on average; steel jet decreases at 63.6 m/s per μs on average; aluminium jet has the largest velocity drop, which is about 233.5 m/s per μs on average.

As for the diameter of the hole on the target, one penetrated by copper jet is close to that by steel jet. Both of them are bigger than the one penetrated by aluminium jet. Among the three materials, copper material has the highest density, moderate sound velocity and good ductility, which is easy to be processed into a given shape. It can produce longer jet with greater penetration capability. On the contrary, the density of aluminium is the lowest. Its fracture strain is less than that of copper and steel. Therefore, the jet generated by aluminium liner fragments more easily, and its penetration capability is the poorest. So the copper is very suitable for shaped charge liner, which can largely destroy all kinds of military equipment protected by armour steel.

To sum up, the material density, ductility, fracture strain have an important effect on the jet formation and penetrating into armour steel. Therefore, the materials of high density and good ductility should be selected as shaped charge liner for penetrating armour steel.

6. CONCLUSIONS

The processes of the jet formation and penetrating a target are studied both experimentally and numerically. Three different liner materials (copper, steel, and aluminium) are selected in this investigation.

(i) The whole process including the detonation of the explosive, the collapse of the liner, jet formation and target penetration is integrated in the simulation. Such integrated numerical simulating approach is of significant practical value for the optimization design of shaped charge.

(ii) The simulated results of jet formation with three different liner materials show that the tip velocity of the jet produced by aluminium liner is the largest, the one by copper liner comes next and the one by steel liner is the smallest. The numerical results are in agreement with the experiment results very well.

(iii) Aluminium jet impacts the target at the largest velocity; but its penetration capability is the poorest. This is due to the fact that the density and the fracture strain of aluminium are the smallest. The tip velocity of the jet produced by the steel liner is the smallest. However, since the density of steel is much larger than that of aluminium, it penetrates the target with a bigger hole and its unit velocity drop is much smaller. The tip velocity of the jet produced by copper liner is faster than that of steel jet but much slower than that of aluminium jet. However, since copper has the largest density and elongation, the unit velocity drop of copper jet is the smallest and its penetration capability is the strongest.

REFERENCES

1. Feng, D.L.; Liu, M.B.; Li, H.Q. & Liu, G.R. Smoothed particle hydrodynamics modeling of linear shaped charge with jet formation and penetration effects. *Comput. Fluids*, 2013, **86**, 77-85. doi: 10.1016/j.compfluid.2013.06.033
2. Held, M. Shaped charge optimization against ERA targets. *Propell. Explos. Pyrot.*, 2005, **30**(3), 216-223. doi: 10.1002/prep.200500009
3. Li, W.B.; Wang, X.M. & Li, W.B. The effect of annular multi-point initiation on the formation and penetration of an explosively formed penetrator. *Int. J. Impact. Eng.*, 2010, **37**(4), 414–424. doi: 10.1016/j.ijimpeng.2009.08.008
4. Wu, J.; Liu, J.B. & Du, Y.X. Experimental and numerical study on the flight and penetration properties of explosively-formed projectile. *Int. J. Impact. Eng.*, 2007, **34**(7), 1147–1162. doi: 10.1016/j.ijimpeng.2006.06.007
5. Liu, J.T.; Cai, H.N.; Wang, F.C. & Fan, Q.B. Multi scale numerical simulation of the shaped charge jet generated from tungsten-copper powder liner. *J. Phys.*, 2013, **419**, 12045-12053. doi: 10.1088/1742-6596/419/1/012045
6. Johnson, G.R. & Stryk, R.A. Some considerations for 3D EFP computations. *Int. J. Impact. Eng.*, 2006, **32**(10), 1621–1634. doi: 10.1016/j.ijimpeng.2005.01.011
7. Huerta, M. & Vigil, M.G. Design, analysis, and field test of a 0.7m conical shaped charge. *Int. J. Impact. Eng.*, 2006, **32**(8), 1201–1213.\ doi: 10.1016/j.ijimpeng.2004.10.002
8. Lee, W.H. Oil well perforator design using 2D Eulerian code. *Int. J. Impact. Eng.*, 2002, **27**(5), 535–559. doi: 10.1016/S0734-743X(01)00054-9
9. Molinari, J.F. Finite element simulation of shaped charges. *Finite Elem. Anal. Des.*, 2002, **38**(10), 921–936. doi: 10.1016/S0168-874X(02)00085-9
10. Chen, Q.Y. & Liu, K.X. A high-resolution Eulerian method for numerical simulation of shaped charge jet including solid–fluid coexistence and interaction. *Comput. Fluids*, 2012, **56**, 92-101. doi: 10.1016/j.compfluid.2011.11.017
11. Baêta-Neves, A.P. & Ferreira, A. Shaped charge simulation using SPH in cylindrical coordinates. *Eng. Computation*, 2015, **32**(2), 370-386. doi: 10.1108/EC-09-2013-0221
12. Ma, S.; Zhang, X.; Lian, Y.P. & Zhou, X. Simulation of high explosive explosion using adaptive material point method. *CMES-Comp. Model. Eng.*, 2009, **39**(2), 101–123.
13. Wang, C.; Ma, T.B. & Ning, J.G. Tracking method for multi-material interfaces and its application in shaped charge. *J. Comput. Theor. Nanos.*, 2008, **5**(8), 1512–1516. doi: 10.1166/jctn.2008.813
14. Johnston, M. & Lim, S. Numerical observation of the jet flight patterns of linear shaped charges. *Appl. Sci.*, 2012, **2**, 629-640. doi: 10.3390/app2030629
15. Wojewodka, A. & Witkowskia, T. Methodology for simulation of the jet formation process in an elongated shaped charge. *Combust. Explo. Shock*, 2014, **50**(3), 362-

367.
doi: 10.1134/S0010508214030150

16. Scott Stewart, D.; Glumac, N.; Najjar, F.M. & Szuck, M.J. Hydrodynamics computation of jet formation and penetration for micro-shaped charges. *Procedia Engineering*, 2013, **58**, 39-47.
doi: 10.1016/j.proeng.2013.05.007
17. Liang, Z.F.; Hu, H.X.; Sun, J. & Lei; Q.H. Numerical simulation and experimental study on the effect of jet penetrating into disconnected targets. *Explo. Shock waves,* 2002, **22**(4), 381-386.
18. Ma, T.B.; Wang, C. & Ning, J.G. Multi-material Eulerian formulations and hydrocode for the simulation of explosions. *Comput. Model. Eng. Sci.*, 2008, **33**(2), 155–178.
19. Libersky, L.; Petschek, A.G.; Carney, T.C.; Hipp, J.R. & Allahdadi, F.A. High strain Lagrangian hydrodynamics-a three-dimensional SPH code for dynamics material response. *J. Comput. Phys.*, 1993, **109**(1), 67–75.
doi: 10.1006/jcph.1993.1199

ACKNOWLEDGMENTS

This research is supported by the National Natural Science Foundation of China under grants 11325209 and 11221202, and the Foundation of State Key Laboratory of Explosion Science and Technology (Grant No. ZDKT11-01).

CONTRIBUTORS

Dr Cheng Wang received his PhD from Beijing Institute of Technology in 2001, presently working as a Professor and doctoral supervisor atState Key Laboratory of Explosion Science and Technology, Beijing Institute of Technology.His research was supported by the National Science Foundation for Distinguished Young Scholars of China in 2013. His area of research is explosion mechanics.

In current study Dr Cheng Wang designed the experiment and developed the computational method.

Mr Jianxu Ding is pursuing his PhD at the Department of Mechanics Engineering of Beijing Institute of Technology. His area of research is explosion mechanics.

In current study Jianxu Ding compiled the codes and analyzed the numerical results.

Mr Haitao Zhao obtained his PhD from Beijing Institute of Technology in 2014. Currently, he is working as research fellow at the Institute of Software Chinese Academy of Sciences. His area of interest is explosion mechanics.

In current study Haitao Zhao performed the experiments and analyzed the obtained data.